Performance of iodine oxides/iodic acids as oxidizers in thermite systems

Tao Wu[a], Xizheng Wang[a], Peter Y. Zavalij[a], Jeffery B. DeLisio[a], Haiyang Wang[b], Michael R. Zachariah[a,b,*]

[a] Department of Chemistry and Biochemistry, University of Maryland, College Park, MD 20742, USA
[b] Department of Chemical and Biomolecular Engineering, University of Maryland, College Park, MD 20742, USA

ARTICLE INFO

ABSTRACT

Iodine oxides are of interest as biocidal components in energetic application such as thermites due to their high energy release and biocidal agent delivery. In this study, various iodine oxides/iodic acids, including I_2O_5, HI_3O_8 and HIO_3, were employed as oxidizers in thermite systems. Their decomposition behaviors were studied using a home-made time resolved temperature-jump/time-of-flight mass spectrometer (T-Jump/TOFMS), which identified a single step decomposition for all oxides at high heating rates ($\sim 10^5$ K/s). In addition, both nano-aluminum (nAl, $\sim$80 nm) and nano-tantalum (nTa, $<$50 nm) were adopted as the fuel in order to fully understand how iodine containing oxidizers react with the fuel during ignition. The ignition and reaction process of nAl-based and nTa-based thermites were characterized with T-Jump/TOFMS, and their combustion properties were evaluated in a constant-volume combustion cell and compared to a traditional thermite system (nAl/CuO). The ignition temperatures of nAl-based thermites using these oxidizers were all very close to the melting point of aluminum ($\sim$660 °C), which suggests that the mobility of the aluminum core dominats the ignition/reaction and the gaseous oxygen released from the decomposition of the oxidizer does not participate in the ignition until the molten aluminum is available. Unlike nAl-based thermites, the ignition temperatures of nTa-based thermites are lower than the oxygen release temperatures from the corresponding bare oxidizers. All nTa-based thermites ignited prior to the release of gas phase oxygen. In this case, a condensed phase reaction mechanism is proposed to dominate the ignition process. Moreover, combustion cell tests results show that nAl/a-HI_3O_8 has the highest pressurization rate and peak pressure and shortest burn time, and since it also has an iodine content of $\sim$75% as high as I_2O_5 on a per mass basis, this material may be a very promising candidate in biocidal application.

© 2018 Published by Elsevier Inc. on behalf of The Combustion Institute.

1. Introduction

High efficiency neutralization of biological warfare agents has become a major research focus within the United States, in addition to many other countries, due to the increased threat of bioterrorism [1–7]. Preliminary laboratory studies have suggested that an ideal neutralization process should contain not only a high thermal but also long-lasting biocidal agent release [8–14]. The main problem with conventional energetic materials is low neutralization efficiency since a thermal neutralization mechanism is dominant in this case [8]. Therefore, it has been proposed that simultaneously delivering a rapid thermal pulse with a remnant

biocidal agent would prolong the exposure time and improve the inactivation process [15]. Halogens-based energetic materials show the most promise because of their excellent biocidal properties [16] when compared to silver-containing energetic materials [17–19]. To incorporate halogens in energetic materials, one can either directly add halogens into the system or assemble halogens into the oxidizers [16,20]. Wang et al. incorporated iodine molecules into Al/CuO thermite systems and found that the Al/CuO/I_2 thermite reaction rate was significantly decreased with increasing the iodine content [21]. Guerrero et al. also showed that mechanical incorporation of iodine into aluminum severely decreases the reaction rate of Al/metal oxides mixtures and even resulted in failed ignition of Al·I_2/Fe_2O_3 [22]. In addition, Dreizin et al. employed mechanically alloyed aluminum–iodine composites as a replacement of aluminum as a fuel additive in energetic formulations and the ignition and combustion tests of those fuels in air indicated that higher iodine concentration lowers ignition tem-

peratures but did not affect the combustion temperatures substantially [14]. They also found improvements in terms of pressurization rate and maximum pressure at constant volume with 15 wt.% and 20 wt.% of I_2 [14]. Furthermore, an effective inactivation of aerosolized spores were achieved using Al/I_2 and $Al/B/I_2$ composites with 15–20 wt.% of iodine [16].

Another approach is to use iodine-containing oxy-compounds that can release HI or I_2 when used as an oxidizer [23]. Iodine-containing oxy-compounds can be broken down into two main categories: metal iodates and iodine oxides/iodic acids. The metal iodates, $AgIO_3$ [8,24], $Bi(IO_3)_3$ [25], $Cu(IO_3)_2$ [15], $Fe(IO_3)_3$ [15] etc., have been previously investigated. One issue with employing metal iodates in thermites is that part of the produced I_2 vapor (all for $AgIO_3$) may react with the product metal particles to form corresponding metal iodides, which lowers the effective iodine content in the metal iodate-based thermite systems. Unfortunately, there are only a limited number of iodine oxides/iodic acids which are relatively stable and obtainable. These include I_2O_5, I_4O_9, HI_3O_8, HIO_3, H_5IO_6, etc. [26–28]. Among these compounds, I_2O_5 (~76% iodine mass fraction) is the most studied in thermite systems [29–33]. In these studies, aluminum particles with different sizes were chosen as the fuel due to its high reaction enthalpy, thermal conductivity and availability. With reported propagation velocities of up to ~2000 m/s for loose ball-milled nAl and nano-scaled I_2O_5 (~10 nm) [32], I_2O_5 shows its high potential in aluminum-based thermites as an extremely aggressive oxidizer. Constant volume combustion tests also show $nAl/micro-I_2O_5$ outperforms traditional aluminum-based thermites such as Al/CuO and Al/Fe_2O_3 [33]. A pre-ignition reaction was proposed as the ignition trigger in which ionic I_2O_5 fragments diffused into the alumina passivation shell of aluminum and to create some reactive complexes exothermically [31,34]. However this mechanism is far from clear as Smith et al. reported that a pre-ignition reaction was not found for aluminum/nano crystalline I_2O_5 reaction in contrast to nano amorphous I_2O_5 case [35].

Recently, Smith et al. reported that a minimum of 150% increase in flame speed was found for $Al/amorphous\ I_4O_9$ compared with Al/I_2O_5 indicating I_4O_9 has more reactive potential than I_2O_5 as an oxidizer when combined with aluminum [36]. Other iodine-containing oxy-compounds have received comparatively much less attention due to their relatively lower iodine content and availability. Nevertheless, their iodine content is still much higher than metal iodates or per-iodates on a per mass basis. This is particularly so for HI_3O_8, which has an iodine content of ~75% and very close to the 76% for I_2O_5. Currently no comparative study examining how the aforementioned iodine oxides/iodic acids perform as oxidizers in thermites system is available. Moreover, we have recently reported that iodine oxides/iodic acids with different particles' sizes can be prepared via either aerosol spray pyrolysis (ASP) or thermal treatment [37,38], making a variety of these materials readily available.

Most of the focus on reactive studies of oxidizers has focused on Aluminum as the fuel. Aluminum has a passivating alumina shell that stabilized the material at ambient conditions. However once the aluminum core reaches near the melting temperature, it can diffuse through the oxide shell and interact with any available oxidizer leading to ignition [39]. To explore the fuel melting aspect of ignition, we also explore in the paper tantalum as a fuel because it has a melting point of ~3000 °C, and thus would not be melted at the point of ignition.

In this paper, we examine the performance of various iodine oxides/iodic acids (I_2O_5, HI_3O_8 and HIO_3) as oxidizers in nAl-based and nTa-based thermites system. Iodine-containing oxides/acids were prepared via an ASP method following procedures in our previous work [37]. Time-resolved temperature-jump time-of-flight mass spectrometer (T-Jump/TOFMS) was used to study the ignition

and decomposition of nAl-based and nTa-based thermites. A high-speed camera simultaneously captured optical emission from the ignition/reaction of the thermites allowing for the ignition time, and corresponding ignition temperature. In addition, constant volume combustion cell tests were performed on aluminum-based thermites.

2. Experimental

2.1. Materials

The aluminum nanopowders (nAl) (Alex, ~80 nm) were purchased from Novacentrix. The active Al was 81% by mass, determined by TGA. Nano-tantalum powders (nTa, <50 nm) were purchased from Global Advanced Metals, with 70% of the mass. Iodic acid ($c-HIO_3$) (99.5 wt %), iodine pantoxide ($c-I_2O_5$), CuO nanoparticles ($n-CuO$, <50 nm) and micro-sized CuO powders ($m-CuO$) purchased from Sigma-Aldrich were directly used as received ("c" represents commercial product; "n" and "m" represents nano-scaled and micro-scaled sizes, respectively). All other chemicals were of analytical grade and were used as purchased without further treatment.

2.2. Preparation of iodine oxides/iodic acids particles

Small-sized (<1 μm) particles of oxides includes $\delta-HIO_3$, $a-HI_3O_8$ and $a-I_2O_5$ were synthesized via aerosol spray pyrolysis (ASP). Here, "a" represents ASP and "δ" refers to HIO_3 with a delta phase. Detailed information on the ASP synthesis method has been previously described [37]. Briefly, 100 mL iodic acid solution (10 mg/mL) was aerosolized (~1 μm in diameter) with a homemade pressure atomizer (~35 psi pressure air) and passed through a silica-gel diffusion drier to remove water. The dry particles are then passed through a tube furnace for chemical conversion. The furnace temperature was set at ~230 and ~375 °C to obtain either $\delta-HIO_3$ or $a-I_2O_5$, respectively with a residence time of about 1 s. For both $\delta-HIO_3$ and $a-I_2O_5$, silica-gels were regenerated at 50 °C. We find that $\delta-HIO_3$ can be obtained within a large range of temperature from 210 to 250 °C. In addition, $a-HI_3O_8$ was obtained with a tube furnace temperature ~250 °C with a silica-gel regeneration temperature of ~80 °C. The final product was collected on a Millipore membrane filter (0.4 μm pore). HI_3O_8 was also prepared via thermal treatment of commercial HIO_3 at ~180 °C and labeled as $t-HI_3O_8$. The final product was characterized by scanning electron microscopy (SEM, Hitachi, SU-70 FEG-SEM) and powder X-ray diffraction (XRD, Bruker D8 Advance using Cu Kα radiation).

2.3. Preparation of thermites

Physically mixed stoichiometric mixtures of nAl and nTa with $\delta-HIO_3$, $c-HIO_3$, $a-HI_3O_8$, $t-HI_3O_8$, $a-I_2O_5$, $c-I_2O_5$, and CuO were based on the following equations. The mixtures were sonicated in dry hexane for 30 min, and left uncapped at room temperature in a low-pressure desiccator to evaporate the solvent. All of the samples employed in this work were stored in a sealed desiccator for future use. Below we list the stoichiometric relations used to prepare the mixture ratios and the associated enthalpy of reactions.

$$4Al + 2HIO_3 \rightarrow I_2 + 2Al_2O_3 + H_2,\ \Delta H_{theoretical} = -2413\ KJ/mol$$

$$32Al + 6HI_3O_8 \rightarrow 9I_2 + 16Al_2O_3 + 3H_2,$$
$$\Delta H_{theoretical} = -20721\ KJ/mol$$

$$10Al + 3I_2O_5 \rightarrow 3I_2 + 5Al_2O_3,\ \Delta H_{theoretical} = -6740\ KJ/mol$$

$$2Al + 3CuO \rightarrow 3Cu + Al_2O_3, \ \Delta H_{theoretical} = -1109 \ KJ/mol$$

$$12Ta + 10HIO_3 \rightarrow 5I_2 + 6Ta_2O_5 + 5H_2,$$
$$\Delta H_{theoretical} = -9059 \ KJ/mol$$

$$32Ta + 10HI_3O_8 \rightarrow 15I_2 + 16Ta_2O_5 + 5H_2,$$
$$\Delta H_{theoretical} = -26515 \ KJ/mol$$

$$2Ta + I_2O_5 \rightarrow I_2 + Ta_2O_5, \ \Delta H_{theoretical} = -1745 \ KJ/mol$$
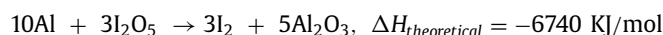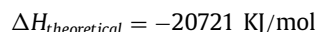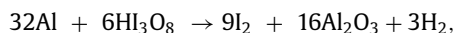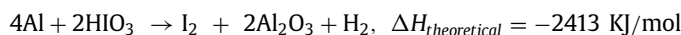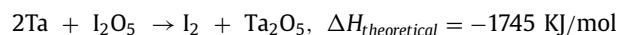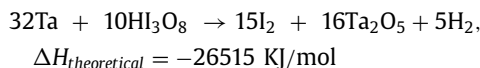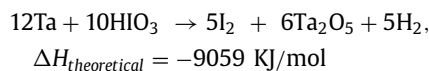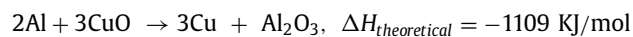
2.4. X-ray diffraction (XRD) measurement and Rietveld refinement

The as-prepared samples were characterized by powder X-ray diffraction. Diffraction pattern was measured using Cu Kα radiation in Bragg–Brentano geometry on Bruker D8 Advance powder diffractometer equipped with incident beam Soller slits, Ni β-filter and LynxEye position sensitive detector. Data were collected from 10° to 90° 2θ with a step size of 0.01578° and counting time of 1 s/step (total exposure time of 180 s/step). The crystal structures were refined by Rietveld method using the Topas software [38].

2.5. T-Jump/TOFMS measurement and high-speed imaging

The decomposition of each oxide listed above was investigated using T-Jump/TOFMS [8]. Typically, a ~1 cm long platinum wire (76 μm in width) with a thin coating of oxidizer sample was rapidly joule-heated to about 1200 °C by a 3 ms pulse at a heating rate of ~10^5 °C/s. The current and voltage signals were recorded, and the temporal temperature of the wire was determined using the Callendar–Van Dusen equation [40]. Spectra were collected at 0.1 ms intervals. The detailed experimental set-up has been previously described [8,40].

In order to experimentally determine the ignition temperature for each thermite, a high speed camera (Vision Research Phantom v12.0) was used to record the optical emission from combustion on the wire during heating. Ignition temperatures of thermite reactions in vacuum were measured from the correlation of optical emission from high speed imaging and temporal temperature of the wire, and were further analyzed in combination with the temporal mass spectra. Each experiment was repeated 3 times.

2.6. Combustion cell test

Combustion properties of themites were evaluated in a constant-volume combustion cell, with simultaneous pressure and optical emission measurements. In this study, 25 mg of thermite powders was loaded inside the cell (constant volume, ~13 cm^3) and ignited by a resistively heated nichrome wire. The temporal pressure and optical emission from the thermite reaction were measured using a piezoelectric pressure sensor and a photodetector, respectively. More detailed information on the combustion cell test can be found in our previous publications [8,40]. Each experiment was repeated at least 3 times.

3. Results and discussion

Various iodine oxides/iodic acids were prepared via ASP using a previously described synthesis method [37]. All of the as-prepared iodine-containing oxides including a-I$_2$O$_5$, δ-HIO$_3$ and a-HI$_3$O$_8$ have an average particle size of about 1 μm with a relatively wide size distribution [37]. SEM images, XRD patterns and TGA/DSC results are published in our previous work [37,38]. Commercial I$_2$O$_5$

Table 1

Crystalline compositions of all the samples employed in Fig. S6 determined by Rietveld refinement of the corresponding XRD pattern.[a]

Samples	Crystalline phases	Samples	Crystalline phases[b]
a-HI$_3$O$_8$	91% HI$_3$O$_8$[c] 9% δ-HIO$_3$[d]	Al/a-HI$_3$O$_8$	89% HI$_3$O$_8$ 11% δ-HIO$_3$
t-HI$_3$O$_8$	100% HI$_3$O$_8$	Al/t-HI$_3$O$_8$	87% HI$_3$O$_8$ 13% δ-HIO$_3$
δ-HIO$_3$	100% δ-HIO$_3$	Al/δ-HIO$_3$	88% δ-HIO$_3$ 12% α-HIO$_3$[e]
c-HIO$_3$	89% α-HIO$_3$ 11% HI$_3$O$_8$	Al/c-HIO$_3$	75% α-HIO$_3$ 25% HI$_3$O$_8$
a-I$_2$O$_5$	91% I$_2$O$_5$[f] 9% δ-HIO$_3$	Al/a-I$_2$O$_5$	68% I$_2$O$_5$ 32% δ-HIO$_3$
c-I$_2$O$_5$	100% HI$_3$O$_8$	Al/c-I$_2$O$_5$	100% HI$_3$O$_8$

[a] Detailed results of Rietveld refinement are included in electronic supporting information as an appendix.
[b] Aluminum signal was found in all Al-based samples and its composition ratio is excluded here for comparison purpose.
[c] PDF# 01-075-3387 HI$_3$O$_8$ [27].
[d] XRD information of δ-HIO$_3$ could be found in [38].
[e] PDF #01-079-1633 HIO$_3$ [41].
[f] PDF #01-082-2225 I$_2$O$_5$ [42].

and HIO$_3$ (labeled as c-I$_2$O$_5$ and c-HIO$_3$) and t-HI$_3$O$_8$ prepared via thermal treatment of c-HIO$_3$ were employed as comparisons. The average particle size of c-I$_2$O$_5$ and c-HIO$_3$ are ~30 μm and t-HI$_3$O$_8$ particles have an average size ~4 μm (Fig. S1). To verify the actual compositions of c-I$_2$O$_5$, c-HIO$_3$ and t-HI$_3$O$_8$, XRD and TGA results shown in Figs. S2 and S3 indicate that c-HIO$_3$ is pure HIO$_3$, c-I$_2$O$_5$ has mostly hydrated (~80%) to HI$_3$O$_8$ and t-HI$_3$O$_8$ is pure HI$_3$O$_8$. As control experiments, nano-sized (<50 nm) and micro-sized (<5 μm) CuO were also included in this work.

T-Jump/TOFMS (3 ms, heating rate ~5 × 10^5 °C /s) was employed to study the initial events of bare oxides or thermites under rapid heating rates, enabling us to probe the reaction process on a time scale close to that of a combustion event. Figure 1A shows the temporal evolution of elemental iodine and O$_2$ from a-HI$_3$O$_8$ during rapid heating. Iodine and O$_2$ are released at approximately the same temperature (~475 °C) indicating that it could be a good candidates for a molecular iodine-releasing oxidizer. The single peak in the species vs. time plots of both Iodine and O$_2$ suggests that a one-step decomposition of a-HI$_3$O$_8$.

To further explore its decomposition, time-resolved mass spectra from rapid heating of a-HI$_3$O$_8$ at 0.8–1.5 ms are shown in Fig. 1B. For mass spectra taken at $t < 1.1$ ms (before the decomposition of the oxidizer), H$_2$O$^+$ (m/z 18), OH$^+$ (m/z 17) and N$_2^+$ (m/z 28) are attributed to the background. Above the decomposition temperature (>1.2 ms), O$_2^+$ and I$^+$ are detected in addition to IO$^+$, IO$_2^+$, I$_2^+$, and I$_2$O$^+$. The appearance of these species implies that the high heating rate decomposition pathway does not go directly to the thermodynamic end product of molecular iodine and oxygen under the conditions of this experimental setup. The temporal profile of those oxygen-containing species is shown in Fig. S4 in which O$_2^+$ has the highest signal intensity. All other iodine oxides/iodic acids have similar time-resolved mass spectra as depicted in Fig. S5.

To evaluate the performance of the iodine oxides/iodic acids as oxidizers in thermite systems, physical mixtures with nAl were made with 30 min sonication of nAl and iodine oxides/iodic acids in dry hexane. To indicate whether the mixing process has any influence on iodine oxides/iodic acids, XRD and TGA were performed and results of iodine oxides/iodic acids before and after mixing shown in Figs. S6 and S7. To be more specific about the exact compositions of each sample in Fig. S6, Rietveld refinement was run for all the XRD patterns and the results are shown in Table 1. Almost for all the samples except for c-I$_2$O$_5$, a small portion of the original compounds either changed to another phase or dehydrated. As the

A

B
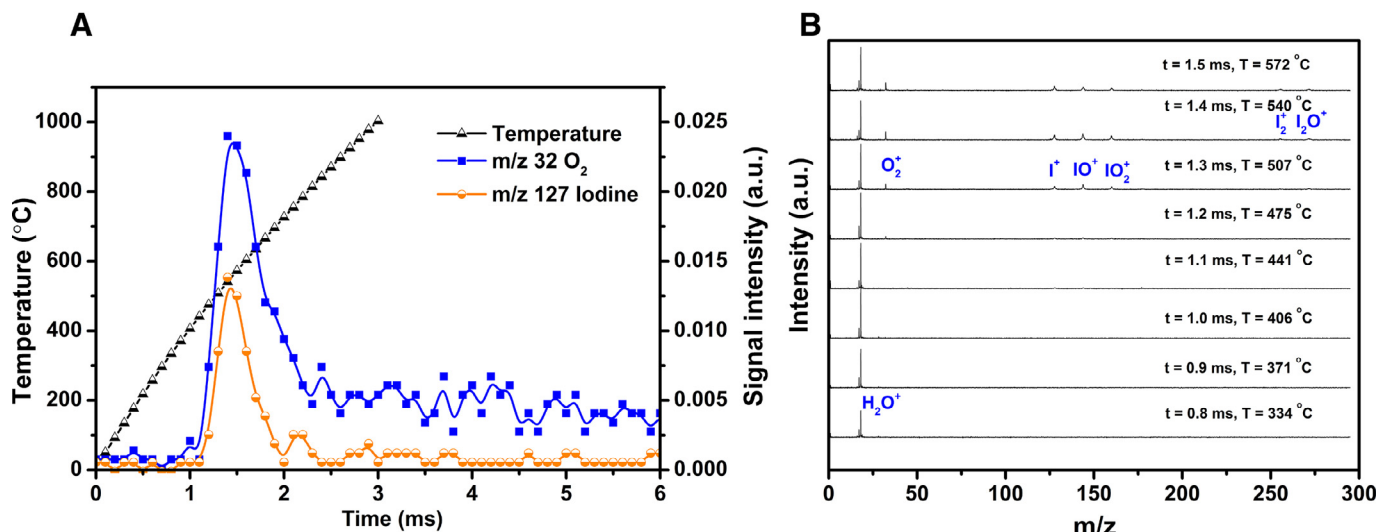
Fig. 1. Representative plot showing the temporal profile of oxygen and iodine upon heating a-HI$_3$O$_8$ when heated at $\sim 5 \times 10^5$ °C/s (A); time-resolved mass spectra of a-HI$_3$O$_8$ (B).

most hygroscopic one among those samples, a-I$_2$O$_5$ made the most changes ($\sim$25% dehydrate into δ-HIO$_3$). Due to the sensitivities of those iodine-containing compounds to water, those minor changes could be resulted from preparation, characterization and/or handling. In addition, the TGA results shown in Fig. S7 show no discernable effect of the thermite preparation process on the hydration state of the iodine oxides/iodic acids. As an example, the SEM images of a-HI$_3$O$_8$ and Al/a-HI$_3$O$_8$ shown in Fig. S8 further indicate that the mixing procedure does not influence the particle size or morphologies of the iodine oxides/iodic acids.

Figure S9 shows some selected temporal snapshots of the Al/a-HI$_3$O$_8$ thermite reaction under vacuum of the T-Jump/TOFMS chamber. Optical emission from reaction was first observed at 1.65 ms, corresponding to a wire temperature of $\sim$664 °C, indicating ignition of nAl/a-HI$_3$O$_8$ thermite. Overall, the optical emission of nAl/a-HI$_3$O$_8$ is not very strong [39] which suggests lower heat generation from the nAl-based thermite [43]. These snapshots also provide an alternative method to roughly determine burn time, calculated to be $\sim$1.2 ms, and will be discussed more in the combustion test results.

From the T-Jump TOFMS results, we found that the bare a-HI$_3$O$_8$ releases oxygen at $\sim$475 °C when heated at $\sim 5 \times 10^5$ °C/s. Under the same heating condition, the nAl/a-HI$_3$O$_8$ thermite showed oxygen appearance at $\sim$575 °C and thus 100 °C higher than the oxygen release temperature of the bare oxidizer (Fig. 2A). This result is quite different from the most of Al/metal oxides thermites where oxygen release from the metal oxide is not influenced by the presence of aluminum fuel [44]. One exception we know of is Al/Bi$_2$O$_3$, which releases oxygen at a temperature that is 700 °C lower than that of the bare Bi$_2$O$_3$ [45]. This effect is the opposite of nAl/a-HI$_3$O$_8$. In this case, the interaction between the iodine ions of a-HI$_3$O$_8$ and the alumina shell of the fuel might form stable alumino-oxy-halides that delay the decomposition of the oxide [31,46].

Even though the oxygen release temperature from nAl/a-HI$_3$O$_8$ thermite increased in comparison to the neat oxide, it is still lower than its ignition temperature ($\sim$664 °C). In fact it is sufficient close to aluminum melting point to reasonable argue that aluminum mobility into aluminum oxide is the initiation process. Clearly gaseous oxygen release from a-HI$_3$O$_8$ at $\sim$575 °C did not initiate ignition. [47]. In fact, Al/Bi$_2$O$_3$, Al/SnO$_2$, Al/AgIO$_3$, Al/CuO and Al/KClO$_4$ also ignited in vacuum at about the melting temperature of aluminum no matter what the oxygen release temperature

is [44]. In addition, the ignition temperature of nAl/a-HI$_3$O$_8$ thermite in Ar environment with a 1 atm pressure was also obtained and it was decreased $\sim$30 °C compared with that in vacuum. Considering the experimental uncertainty of $\pm$50 °C, it is reasonable to say that the ignition temperatures of nAl/a-HI$_3$O$_8$ in vacuum and 1 atm Ar are roughly the same, which again implies the importance of the melting phase transition of aluminum fuel.

If we consider Al/Co$_3$O$_4$, which has an ignition temperature of $\sim$1095 °C, and is higher than its oxygen release temperature and the melting point of aluminum [44]. In this case, the generated gas phase oxygen also has no correlation with its ignition. However, the nAl/a-HI$_3$O$_8$ ignited right after the aluminum melted. We have previously investigated the ignition of nAl in an oxygen environment and found that the ignition temperature decreased with increasing O$_2$ pressure and dropped below the melting point of bulk aluminum at >7.4 atm [47]. Why then does nAl/a-HI$_3$O$_8$ thermite ignite at the melting point of aluminum? Obviously, the partial pressure of O$_2$ during the ignition of nAl/a-HI$_3$O$_8$ thermite under vacuum is much lower than 7.4 atm. We have shown in prior work that the oxygen concentration in solid oxidizers (7 $\times$ 10^4 mol/m^3) is much higher than that in gas (100 mol/ m^3 for 18 atm O$_2$ gas) [47]. Thus, in vacuum, the oxygen pressure around the fuel is likely very high. This is also supported by the combustion cell tests where a high pressurization rate is observed after ignition. Moreover, the local gas phase oxygen released from the oxidizer has a much higher temperature than the free O$_2$ in the pressurized ignition temperature tests described above. Both factors suggest that the gas phase oxygen from the oxidizer might also plays a role in the ignition of thermites.

Time-resolved mass spectra taken at 0.1 ms intervals from a nAl/a-HI$_3$O$_8$ thermite reaction is shown in Fig. 2A. As we expected, O$_2^+$, I$^+$ and I$_2^+$ peaks were first observed at a time of about 1.3 ms ($\sim$536 °C), which is prior to ignition, and earlier than IO$^+$ and IO$_2^+$ species appeared. At the ignition temperature, IO$^+$ and IO$_2^+$ concentration also diminished, which implies that those intermediate iodine sub-oxide species also took part in the aluminum combustion [33].

Reactions between solids are by their nature limited by the movement of component reactive species or fragments. To further investigate the role of these oxidizers in the thermite reaction, a fuel was chosen that unlike aluminum would be immobile at least at the point of ignition. Aluminum was replaced with tantalum as a means to potentially tweeze out the relationship between io-

A

B
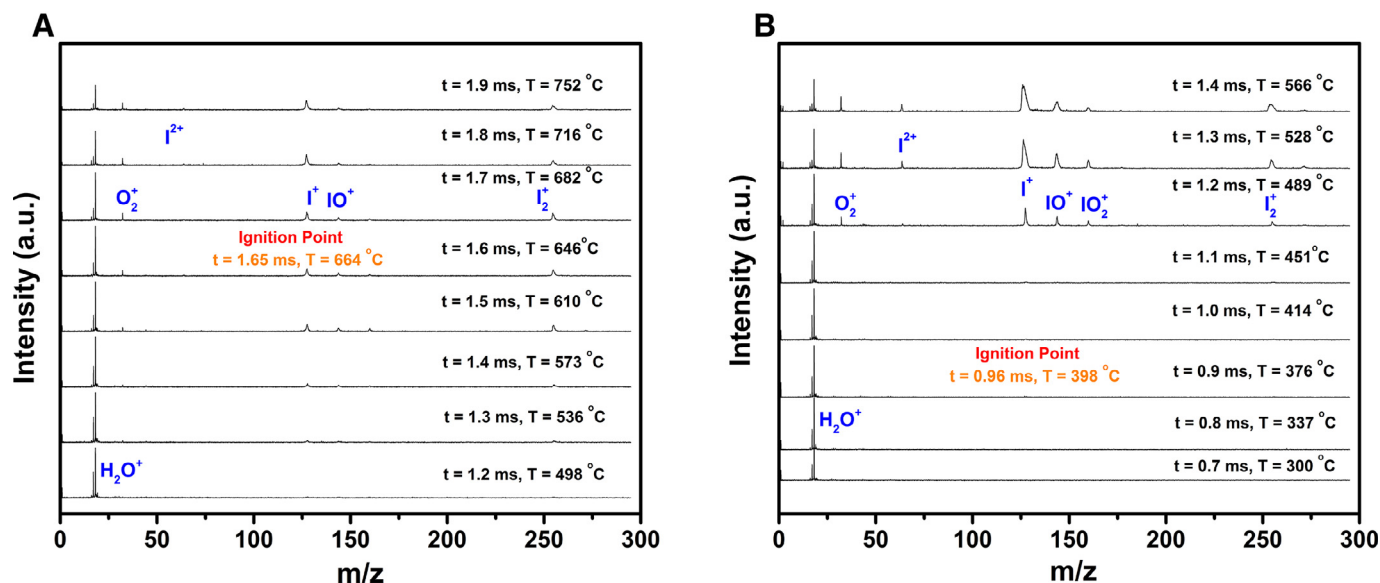
Fig. 2. Time-resolved mass spectra of nAl/a-HI$_3$O$_8$ (A) and nTa/a-HI$_3$O$_8$ (B).
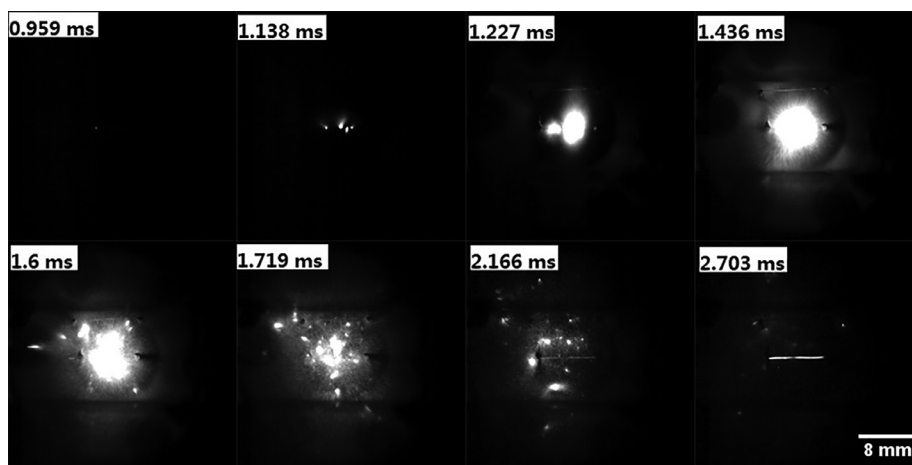
Fig. 3. Sequential snapshots of nTa/a-HI$_3$O$_8$ thermite burning on a high rate heating (5×10^5 °C/s) Pt wire under vacuum, captured by a high speed camera. The labels in each image are the time elapsed after triggering.

dine and oxygen release with ignition. Similar to aluminum, tantalum also has a native oxide shell (Ta$_2$O$_5$). However, tantalum has a very high melting point of about 3017 °C, which rules out the influence of the melting phase transition in the scope of ignition temperature test, which reaches a maximum wire temperature of ~1200 °C. Sequential snapshots of the nTa/a-HI$_3$O$_8$ thermite reaction during rapid heating under vacuum were captured using a high speed camera and are shown in Fig. 3. In contrast to nAl/a-HI$_3$O$_8$, the nTa/a-HI$_3$O$_8$ reaction is surprisingly much more vigorous with strong light emission. The images in Fig. 3 also show that multiple ignition points appeared after ignition and propagate toward each other to ignite the whole thermite. The burn time of nTa/a-HI$_3$O$_8$ is roughly 1.7 ms, which is longer than that of nAl/a-HI$_3$O$_8$. In addition, time-resolved mass spectra of the nTa/a-HI$_3$O$_8$ thermite reaction (Fig. 2B) shows that its oxygen and iodine release temperatures are ~450 °C, which is very close to those of neat a-HI$_3$O$_8$ (~475 °C). However, nTa/a-HI$_3$O$_8$ thermite ignited at ~400 °C (0.96 ms) prior to the oxygen release from the bare oxidizer (~475 °C) and Fig. 2B also shows neither oxygen gas nor elemental iodine are detected before the ignition, which suggests a condensed phase reaction mechanism was dominant. While, considering that T-Jump/TOFMS has a temperature measurement un-

certainty of about ±50 °C [44], it would be also possible that a very small amount of the oxidizer starts decomposing around the ignition temperature that ignites the thermite. As to the condensed phase mechanism, it has been found that cracks on in the oxide shell are formed when tantalum is rapidly heated to above 500 °C due to the amorphous to crystalline phase change of the oxide shell [48]. However, the ignition of nTa/a-HI$_3$O$_8$ occurs ~100 °C earlier than this phase change.

The performance of all the iodine oxides/iodic acids (δ-HIO$_3$, c-HIO$_3$, a-HI$_3$O$_8$, t-HI$_3$O$_8$, a-I$_2$O$_5$ and c-I$_2$O$_5$) as an oxidizer using nAl or nTa as the fuel are summarized in the following figures. Figure 4 shows the relationship between iodine and O$_2$ release temperature in neat iodine oxides/iodic acids, and the ignition temperature of nAl-based and nTa-based thermites. For all iodine oxides/iodic acids, we find that oxygen and iodine occurs at the same temperature which suggests iodine oxides/iodic acids directly decomposed into iodine and oxygen at high heating rate.

All oxidizers when reacting with aluminum ignited about their oxygen release temperature. Moreover, they all ignited around the same temperature under vacuum, and at approximately the melting point of aluminum 660 °C. Those results indicate that the ignition of nAl-based thermites is dominated by the melting of alu-

Table 2
Combustion cell test data for nAl-based thermites with different oxidizers. Each sample was repeated at least three times. All the numbers have a deviation at ~25.

Oxidizers (nAl, stoichiometric)	Peak pressure (Kpa)	Pressurization rate (Kpa/ms)	Burn time (ms)	Peak optical emission (Volts)
n-CuO	405	5653	0.31	2.24
m-CuO	162	157	1.60	2.70
δ-HIO$_3$	281	166	1.39	6.09
c-HIO$_3$	104	6	12.7	0.41
a-I$_2$O$_5$	293	207	1.29	7.52
c-I$_2$O$_5$	156	31	2.49	2.88
a-HI$_3$O$_8$	384	450	0.96	11.7
t-HI$_3$O$_8$	214	175	1.25	7.79
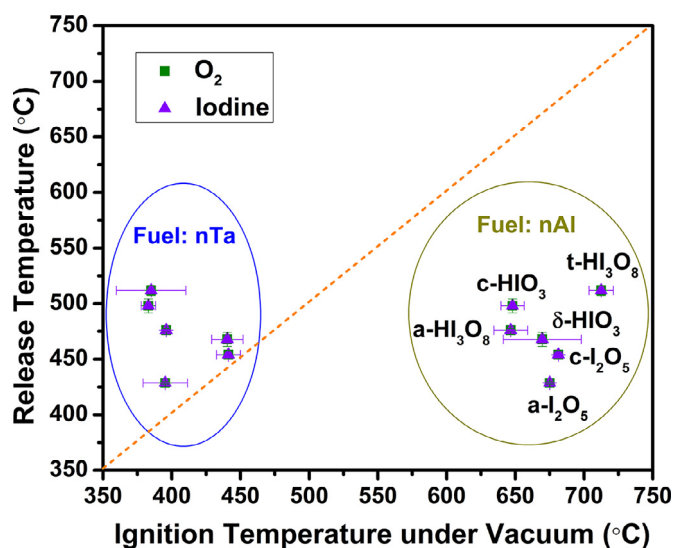
Fig. 4. I and O$_2$ release temperature in neat iodine oxides/iodic acids, and the ignition temperature of corresponding nAl-based and nTa-based thermites under vacuum. Error bars correspond to at least two measurements. The orange dashed line stands for a perfect correlation. (For interpretation of the references to colour in this figure legend, the reader is referred to the web version of this article.)

minum. Aluminum could then react with oxygen released from the oxidizer, but more likely since this experiment is conducted in vacuum, reacts heterogeneously with the oxidizer, once aluminum becomes mobile.

In contrast to aluminum, when tantalum was employed as the fuel, all nTa-based thermites ignited at temperatures lower than the oxygen release temperatures relative to their corresponding neat oxidizers. Clearly, in this case a condensed phase reaction mechanism is dominant [44]. We have previously found that the Ta$_2$O$_5$ has a preferred orientation during crystalline oxide growth and this crystallization upon rapid heating result in cracking of the oxide shell that may enhance oxygen diffusion [48]. Since this is below the melting point of tantalum the oxygen from the decomposition of iodine oxides/iodic acids diffuse through the Ta$_2$O$_5$ cracked or weakened shell to the tantalum core. Moreover, even though a-HI$_3$O$_8$ and a-I$_2$O$_5$ has a significantly smaller particle size than c-HI$_3$O$_8$ or c-I$_2$O$_5$, their ignition temperatures are essentially within the measurement uncertainty which implies that particle size of the oxidizer is relatively unimportant and that the reaction of tantalum and gaseous O$_2$ contributed to the ignition, in agreement with the ignition of nAl/potassium oxysalts energetic composites [49].

To investigate the combustion performance of iodine oxides/iodic acids as oxidizers in nAl-based thermites at 1 atm, constant volume combustion cell tests were performed on each thermite and the results are summarized in Table 2. Nano-sized copper oxide outperforms micro-sized copper oxide due to the huge

difference between their particle sizes [50]. Given the fact that all iodine oxides/iodic acids include in this work have average particles size larger than 1 μm (~1 μm for δ-HIO$_3$, a-HI$_3$O$_8$ and a-I$_2$O$_5$; ~4 μm for t-HI$_3$O$_8$; ~30 μm for c-HIO$_3$ and c-I$_2$O$_5$), micro-sized copper oxide was chosen to be the control experiment.

Table 2 shows that those iodine oxides/iodic acids prepared via ASP outperform the corresponding commercial samples, with a shorter burn time and higher maximum pressure and pressurization rate. In addition, t-HI$_3$O$_8$ has better performance than c-I$_2$O$_5$, but since they are both really HI$_3$O$_8$ the difference in performance can probably be attributed to the smaller particle size of t-HI$_3$O$_8$. Similar to the nano-sized and micro-sized CuO, particle size plays a very important role in combustion. In our previous work, we attributed the pressurization to the oxygen release from the oxidizer particles [43]. For nAl/micro-oxidizer thermites, the decomposition of the oxidizer is the rate-limiting step that results in the delay of the pressure rise [33,43]. Thus, the particle size of the oxidizer is crucial for a thermite to perform well in combustion cell test because smaller particle size guarantees shorter diffusion length and higher specific surface area and therefore faster heat transfer and shorter the delay time for pressure rise [51]. In other words, the decomposition reaction of commercial iodine oxides/iodic acids that have larger particles size is the rate-limiting step during nAl-based thermites combustion, which results in slower thermite reaction rate and thus relatively poor performance in terms of pressurization rate [50]. Given the fact the only difference between commercial and aerosol synthesized iodine oxides/iodic acids is the particle size, it is reasonable to conclude that the higher pressurization rates and maximum pressures are resulted from the faster heat transfer owing to the higher contact area with employing smaller sized oxidizer particles. However ignition with high heating rate by its nature is essentially the point where the self-heating by exothermic reaction exceeds heat loss and a non-linear reaction event occurs. In this case, the initial heat release from thermite reaction was not affected by oxidizers particles size and thus the ignition temperature is independent on particles size, which is consistent with our previous reports [51,52].

In addition, the fact that t-HI$_3$O$_8$ outperforms c-HIO$_3$ and a-HI$_3$O$_8$ outperforms δ-HIO$_3$ imply that HI$_3$O$_8$ is a better oxidizer. In fact, the pressurization rate and maximum pressure of the nAl/a-HI$_3$O$_8$ thermite reaction are ~450 Kpa/ms and ~384 Kpa, which is significantly above the other oxidizers evaluated, and indicate that the a-HI$_3$O$_8$ is the best gas generator in this study. The nAl/a-HI$_3$O$_8$ thermite reaction shows the highest peak optical emission and the shortest burn time, demonstrating it outperforms others in heat generation rate. Figure 5 shows the direct comparison between the pressure and optical trace of nAl/m-CuO and nAl/a-HI$_3$O$_8$. Based on the combustion behavior, a-HI$_3$O$_8$ seems to warrant further attention for biocidal applications since it features both high pressure generation and energy release and has almost the same iodine content as I$_2$O$_5$ on a per mass basis (I$_2$O$_5$: ~76%; HIO$_3$: ~72%; HI$_3$O$_8$: ~75%). In a prior work it has been reported [53] that I$_2$O$_5$ showed increased reactivity with a polar solvent treatment. Since
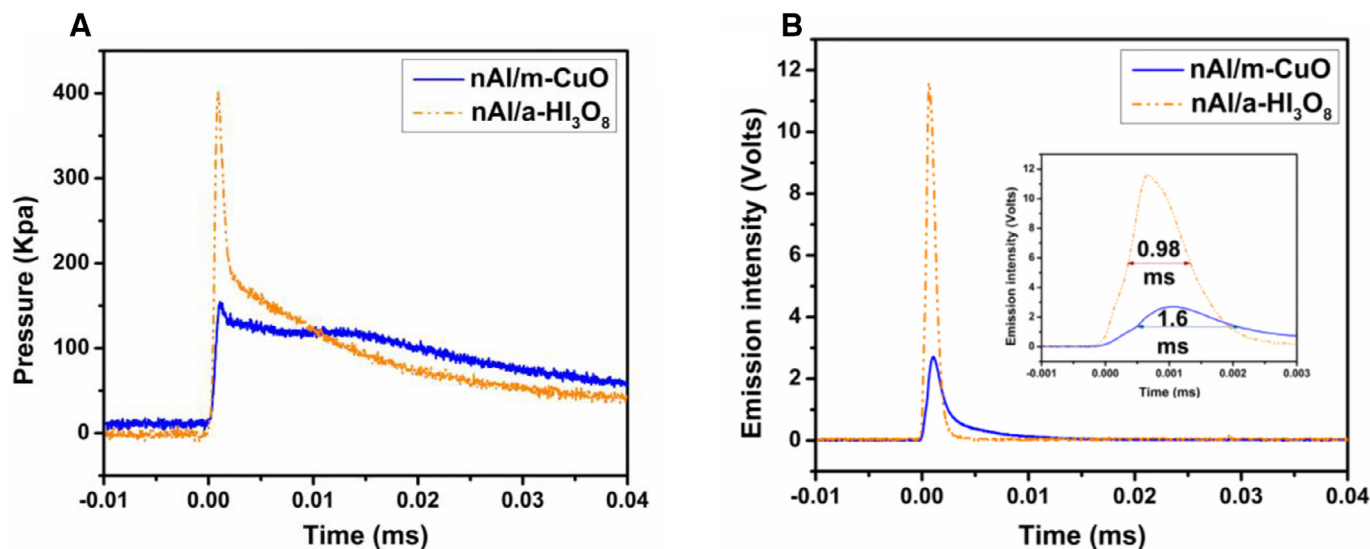
Fig. 5. Direct comparison between the pressure (A) and optical (B) trace of nAl/m-CuO and nAl/a-HI$_3$O$_8$.

I$_2$O$_5$ likely hydrated to form HI$_3$O$_8$ and HIO$_3$ in the polar solvent, it is reasonable to conclude that the results were showing that I$_2$O$_5$ hydrates outperform I$_2$O$_5$ in a flame speed test. This is consistent with our results.

4. Conclusions

In this study, various iodine oxides/iodic acids, including a-I$_2$O$_5$, a-HI$_3$O$_8$ and δ-HIO$_3$, were prepared based on the aerosol route published previously, and were employed as the oxidizer in thermite systems. Their decomposition behavior was studied using T-Jump/TOFMS, which identified a single decomposition step for all oxides at high heating rates compared with the multi-steps process at low heating rate. The ignition temperatures of nAl-based thermites are all ∼650 °C which is at the melting point of aluminum (∼660 °C). This suggests that the mobility of the aluminum core is dominating the ignition/reaction while the gaseous oxygen released from the decomposition of the oxidizer does not participate in the ignition until the molten aluminum was available. Unlike nAl-based thermites, the ignition temperatures of nTa-based thermites are lower than the oxygen release temperatures from the corresponding bare oxidizers. In this case, a condensed phase reaction mechanism is proposed to dominate the ignition process. Combustion tests show that nAl/a-HI$_3$O$_8$ has the highest pressurization rate and peak pressure and shortest burn time, and since it also has an iodine content of ∼75% which is as high as I$_2$O$_5$ on a per mass basis, this material may be a very promising candidate in biocidal application.

Acknowledgments

Supplementary materials

Supplementary material associated with this article can be found, in the online version, at doi:10.1016/j.combustflame.2018.01.017.

References

[1] E.R. Blatchley, A. Meeusen, A.I. Aronson, L. Brewster, Inactivation of Bacilus spores by ultraviolet or gamma radiation, J. Environ. Eng. 13 (2005) 1245.

[2] K.T. Sullivan, C.W. Wu, N.W. Piekiel, K. Gaskell, M.R. Zachariah, Synthesis and reactivity of nano-Ag$_2$O as an oxidizer for energetic systems yielding antimicrobial products, Combust. Flame 160 (2013) 438.

[3] M. Schoenitz, T.S. Ward, E.L. Dreizin, Fully dense nanocomposite energetic powders prepared by arrested reactive milling, Proc. Combust. Inst. 30 (2005) 2071.

[4] K.J. Blobaum, A.J. Wagner, J.M. Plitzko, D. Van Heerden, D.H. Fairbrother, T.P. Weihs, Investigating the reaction path and growth kinetics in CuO$_x$/Al multilayer foils, J. Appl. Phys. 94 (2003) 2923.

[5] K. Zhang, C. Rossi, G.A. Rodriguez, Development of a nAl/CuO based energetic material on silicon substrate, Appl. Phys. Lett. 91 (2007) 113117.

[6] S.M. Umbrajkar, S. Seshadri, M. Schoenitz, V.K. Hoffmann, E.L. Dreizin, Aluminum-rich Al-MoO$_3$ nanocomposite powders prepared by arrested reactive milling, J. Propul. Power 24 (2008) 192.

[7] T.S. Ward, W. Chen, M. Schoenitz, R.N. Dave, E.L. Dreizin, A study of mechanical alloying processes using reactive milling and discrete element modeling, Acta Mater. 53 (2005) 2909.

[8] K. Sullivan, N. Pickiel, S. Chowdhury, C.W. Wu, C. Johnson, M.R. Zachariah, Ignition and combustion characteristics of nanoscale Al/AgIO$_3$: a potential energetic biocidal system, Combust. Sci. Technol. 183 (2011) 205.

[9] W. Zhou, M.W. Orr, V.T. Lee, M.R. Zachariah, Synergistic effects of ultrafast heating and gaseous chlorine on the neutralization of bacterial spores, Chem. Eng. Sci. 144 (2016) 39.

[10] W. Zhou, M.W. Orr, G. Jian, S. Watt, V.T. Lee, M.R. Zachariah, Inactivation of bacterial spores subjected to sub-second thermal stress, Chem. Eng. J. 279 (2015) 578.

[11] F.T. Tabit, E. Buys, The effects of wet heat treatment on the structural and chemical components of Bacillus sporothermodurans spores, Int. J. Food Microbiol. 140 (2010) 207.

[12] S. Zhang, M. Schoenitz, E.L. Dreizin, Mechanically alloyed Al–I composite materials, J. Phys. Chem. Solids 71 (2010) 1213.

[13] S. Zhang, M. Schoenitz, E.L. Dreizin, Iodine release, oxidation, and ignition of mechanically alloyed Al–I composites, J. Phys. Chem. C 114 (2010) 19653.

[14] S. Zhang, C. Badiola, M. Schoenitz, E-L. Dreizin, Oxidation, ignition, and combustion of Al·I$_2$ composite powders, Combust. Flame 159 (2012) 1980.

[15] H. Wang, G. Jian, W. Zhou, J. DeLisio, V. Lee, M-R. Zachariah, Metal iodate-based energetic composites and their combustion and biocidal performance, ACS Appl. Mater. Interfaces 7 (2015) 17363.

[16] Y. Aly, S. Zhang, M. Schoenitz, V.K. Hoffmann, E.L. Dreizin, M. Yermakov, R. Indugula, S.A. Grinshpun, Iodine-containing aluminum-based fuels for inactivation of bioaerosols, Combust. Flame 161 (2014) 303.

[17] C.E. Johnson, K.T. Higa, Iodine rich biocidal reactive materials. Presented at MRS Meeting, vol. 11, Boston (2012), p. 25.

[18] O. Mulamba, E.M. Hunt, M.L. Pantoya, Neutralizing bacterial spores using halogenated energetic reactions, Biotechnol. Bioprocess. Eng. 18 (2013) 918.

[19] C. He, J. Zhang, J.M. Shreeve, Dense iodine-rich compounds with low detonation pressures as biocidal agents, Chem. Eur. J. 19 (2013) 7503.

[20] J.Y. Feng, G.Q. Jian, Q. Liu, M.R. Zachariah, Passivated Iodine pentoxide oxidizer for potential biocidal nanoenergetic applications, ACS Appl. Mater. Interfaces 5 (2013) 8875.

[21] H. Wang, J. Delisio, G. Jian, W. Zhou, M.R. Zachariah, Electrospray formation and combustion characteristics of iodine-containing Al/CuO nanothermite microparticles, Combust. Flame 162 (2015) 2823.

[22] S.E. Guerrero, E.L. Dreizin, E. Shafirovich, Combustion of thermite mixtures based on mechanically alloyed aluminum–iodine material, Combust. Flame 164 (2016) 164.

[23] D. Fischer, T.M. Klapçtke, J. Stierstorfer, Synthesis and characterization of guanidinium difluoroiodate, $[C(NH_2)_3]^+[IF_2O_2]^-$ and its evaluation as an ingredient in agent defeat weapons, Anorg. Allg. Chem. 637 (2011) 660.

[24] X. Hu, W. Zhou, X. Wang, T. Wu, J.B. DeLisio, M.R. Zachariah, On-the-fly green generation and dispersion of AgI nanoparticles for cloud seeding nuclei, J. Nanopart. Res. 18 (2016) 214.

[25] X. Hu, J.B. DeLisio, X. Li, W. Zhou, M.R. Zachariah, Direct deposit of highly reactive $Bi(IO_3)^{3-}$ polyvinylidene fluoride biocidal energetic composite and its reactive properties, Adv. Eng. Mater. (2016), doi:10.1002/adem.201500532.

[26] B.K. Little, S.B. Emery, J.C. Nittinger, R.C. Fantasia, M.C. Lindsay, Physiochemical characterization of iodine (V) oxide, part 1: hydration rates, Propellants Explos. Pyrotech. 40 (2015) 595.

[27] A. Fischer, Redetermination of HI_3O_8, an adduct of formula $HIO_3 \cdot I2O5$, Acta Cryst. E61 (2005) i278.

[28] A. Wikjord, P. Taylor, D. Torgerson, L. Hachkowski, Thermal behavior of corona-precipitated iodine oxides, Thermochim. Acta 36 (1980) 367.

[29] K.S. Martirosyan, Nanoenergetic gas-generators: principles and applications, J. Mater. Chem. 21 (2011) 9400.

[30] B.K. Little, E.J. Welle, S.B. Emery, M.B. Bogle, V.L. Ashley, A.M. Schrand, M.C. Lindsay, Chemical dynamics of nAl/iodine (V) oxide, J. Phys. Conf. Ser. 500 (2014) 052025.

[31] C. Farley, M. Pantoya, Reaction kinetics of nanometric aluminum and iodine pentoxide, J. Therm. Anal. Calorim. 102 (2010) 609.

[32] K.S. Martirosyan, L. Wang, D. Luss, Development of nanoenergetic materials based on Al/I_2O_5 system, NSTI-Nanotech 2 (2010) 137.

[33] G. Jian, S. Chowdhury, J. Feng, M.R. Zachariah, The ignition and combustion study of nano-Al and iodine pentoxide thermite, Proc. Combust. Inst. 2 (2013) 1287.

[34] O. Mulamba, M. Pantoya, Exothermic surface reactions in alumina–aluminum shell–core nanoparticles with iodine oxide decomposition fragments, J. Nanopart. Res. 16 (2014) 2310.

[35] D.K. Smith, K. Hill, M.L. Pantoya, J.S. Parkey, M. Kesmez, Reactive characterization of anhydrous iodine (v) oxide (I_2O_5) with aluminum: amorphous versus crystalline microstructures, Thermochim. Acta 641 (2016) 55.

[36] D.K. Smith, M.L. Pantoya, J.S. Parkey, M. Kesmez, Reaction kinetics and combustion dynamics of I4O9 and aluminum mixtures, J. Vis. Exp. 117 (2016) e54661.

[37] T. Wu, A. SyBing, X. Wang, M.R. Zachariah, Aerosol synthesis of phase pure iodine/iodic biocide microparticles, J. Mater. Res. 4 (2017) 890.

[38] T. Wu, P.Y. Zavalij, M.R. Zachariah, Crystal structure of a new polymorph of iodic acid, HIO_3, from powder diffraction, Powder Diffr. 32 (2017) 261.

[39] G. Jian, N.W. Piekiel, M.R. Zachariah, Time-resolved mass spectrometry of nAl and nAl/CuO thermite under rapid heating: a mechanistic study, J. Phys. Chem. C 116 (2012) 26881.

[40] W. Zhou, J.B. DeLisio, X. Li, L. Liu, M.R. Zachariah, Persulfate salt as an oxidizer for biocidal energetic nano-thermites, J. Mater. Chem. A 3 (2015) 11838.

[41] K. Stahl, M. Szafranski, A single-crystal neutron diffraction study of HIO_3 at 295 and 60 K and DIO_3 at 295 K, Acta Chem. Scand. 46 (1992) 1146.

[42] H. Fjellvag, A. Kjekshus, The crystal structure of I2O4 and its relations to other iodine-oxygen-containing compounds, Acta Chem. Scand. 48 (1994) 815.

[43] K. Sullivan, M.R. Zachariah, Simultaneous pressure and optical measurements of nanoaluminum thermites: investigating the reaction mechanism, J Propul. Powder 26 (2009) 467.

[44] G. Jian, S. Chowdhury, K. Sullivan, M.R. Zachariah, Nanothermite reactions: is gas phase oxygen generation from the oxygen carrier an essential prerequisite to ignition? Combust. Flame 160 (2013) 432.

[45] N. Piekiel, L. Zhou, K.T. Sullivan, S. Chowdhury, G. Eagan, M.R. Zachariah, Initiation and reaction in Al/Bi_2O_3 nanothermites: evidence for the predominance of condensed phase chemistry, Combust. Sci. Technol. 186 (2014) 1209.

[46] M. Toyohara, M. Kaneko, N. Mitsutsuka, H. Fujihara, N. Saito, T. Murase, Contribution to understanding iodine sorption mechanism onto mixed solid alumina cement and calcium compounds, J. Nucl. Sci. Technol. 39 (2002) 950.

[47] W. Zhou, J.B. DeLisio, X. Wang, G. Eagan, M.R. Zachariah, Evaluating free vs. bound oxygen on ignition of nanoaluminum energetics leads to a critical reaction rate criterion, J. Appl. Phys. 118 (2015) 114303.

[48] J.B. DeLisio, G.C. Egan, S.C. Liou, W.A. Chiou, M.R. Zachariah, Probing the oxidation mechanism of Ta nanoparticles via in-situ and ex-situ ultra-fast heating TEM/STEM, Microsc. Microanal. 22 (Suppl 3) (2016) 780–781.

[49] W. Zhou, J.B. Delisio, X. Wang, M.R. Zachariah, Reaction mechanisms of potassium oxysalts based energetic composites, Combust. Flame 177 (2017) 1.

[50] M.R. Weismiller, J.Y. Malchi, J.G. Lee, R.A. Yetter, T.J. Foley, Effects of fuel and oxidizer particle dimensions on the propagation of aluminum containing thermites, Proc. Combust. Inst. 33 (2011) 1989.

[51] E.L. Dreizin, Metal-based reactive nanomaterials, Prog. Energy Combust. Sci. 35 (2009) 141.

[52] G. Egan, K. Sullivan, T. Olson, T. Han, M. Worsley, M.R. Zachariah, Ignition and combustion characteristics of nanoaluminum with copper oxide nanoparticles of differing oxidation state, J. Phys. Chem. C 120 (2016) 29023.

[53] D.K. Smith, J. McCollum, M.L Pantoya, Effect of environment of iodine oxidation state on reactivity with aluminum, Phys. Chem. Chem. Phys. 18 (2016) 11243.